Nano Research

Open Access

Research Article

Deciphering the active site of the hydrogen evolution reaction on metal phthalocyanine-carbon nanotube hybrid catalysts

Bernie T. Wang[1,2], Conor L. Rooney[1,2], Nia J. Harmon[1,2], Kunpeng Yu[1,2], Qi Sun[1,2], and Hailiang Wang[1,2]✉

[1] *Department of Chemistry, Yale University, New Haven, Connecticut 06520, USA*
[2] *Energy Sciences Institute, Yale University, West Haven, Connecticut 06516, USA*

Cite this article: *Nano Research*, **2026**, *19*, 94908427. https://doi.org/10.26599/NR.2026.94908427

ABSTRACT: Electrochemical reduction of CO_2 to methanol is a sustainable method for synthesizing a liquid fuel and feedstock chemical from a cheap and abundant starting material. This reaction can be catalyzed by the hybrid molecular catalyst of cobalt phthalocyanine (CoPc) on carbon nanotubes (CNTs). However, the negative potential needed to produce methanol also gives rise to the hydrogen evolution reaction (HER), compromising Faradaic efficiency and limiting the methanol productivity. Further improvement is constrained by the lack of understanding whether the CoPc molecules or the CNT support is the major active sites for HER. In this work, we distinguish the activity of CoPc for HER by systematically varying the mass loading of CoPc on CNTs. This series of materials, along with materials of nickel phthalocyanine (NiPc) and iron phthalocyanine (FePc) molecules loaded on CNTs, were measured for their HER activity at potentials relevant to CO_2 reduction. At −0.94 V vs. reversible hydrogen electrode (RHE), CoPc molecules are one order of magnitude more active for HER than the CNT support or NiPc/FePc molecules. This demonstrates that the undesirable HER activity of CoPc/CNT is mainly from the CoPc molecules.

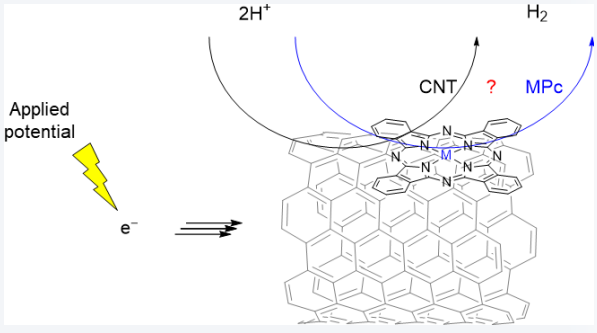

KEYWORDS: electrocatalysis, heterogenized molecular catalyst, CO_2 reduction, H_2 evolution

Electrochemical carbon dioxide (CO_2) conversion to value-added chemicals is an important field of research for renewable energy and sustainable chemical feedstocks. Metal phthalocyanines (MPcs) supported on multiwalled carbon nanotubes (CNTs) are a promising category of CO_2 reduction electrocatalysts, as the MPc molecular structure allows for tunability [1] while the CNT support lends advantages of heterogeneous catalysts such as high current density and separability [2, 3]. In particular, CoPc/CNT has been reported to catalyze CO_2 electroreduction to CO [4, 5] as well as further reduction to methanol [6–9], an important liquid product. Other MPcs such as NiPc and FePc have been found to be active for catalyzing CO_2 conversion, mostly to CO [10–13].

Because CO_2 electroreduction reactions always occur at reductive electrode potentials and in most cases in the presence of protons, the hydrogen evolution reaction (HER) is almost always a competing reaction. This becomes more dominant at more negative potentials. For example, CO_2 reduction to methanol catalyzed by CoPc/CNT happens at −1 V vs. the reversible hydrogen electrode (RHE, all potentials in this work are referenced to RHE unless otherwise stated) in neutral electrolyte, where HER is a considerable side reaction limiting the methanol Faradaic efficiency (FE) below 50% [7]. Understanding HER on CoPc/CNT catalyst materials is therefore crucial for further improvement of CO_2 conversion to methanol. Generally speaking, HER can occur on the CoPc molecules and/or on the CNT support (Fig. 1). Reactions on these two types of sites may go through different mechanisms and require different strategies to suppress. However, up to now, there has been no report of a good way to tell these two paths apart, and the differentiation of HER occurring at CoPc vs. CNT sites is still yet to be done.

Herein we studied the differing activities of MPc and CNT for HER. We systematically varied the amount of molecular catalyst loaded onto CNTs, as the nearly molecular-level dispersion of MPc on the CNT surface allows MPc coverage to increase linearly with mass loading. These varied-loading materials were tested electrochemically to generate activity measurements, which can then be used to deconvolute the contributions of MPc vs. CNT toward HER. We find that all three of the MPcs (CoPc, NiPc, and FePc), when the reaction rate is not limited by mass transport, exhibit a linear relationship between mass loading and current

Received: August 29, 2025; **Revised:** January 9, 2026
Accepted: January 10, 2026

✉Address correspondence to hailiang.wang@yale.edu

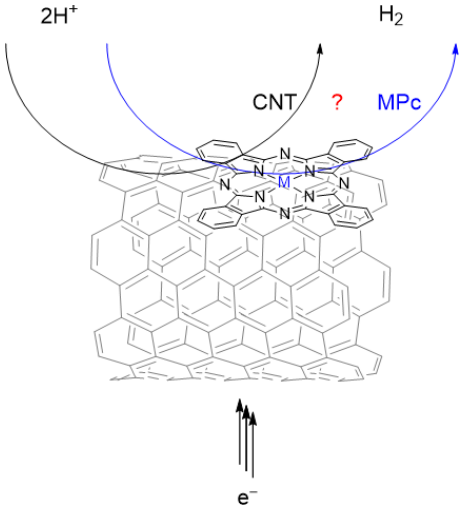

Figure 1 Scheme of different sites of HER. Electrons are fed to the system by applying potential bias. Protons from solution may react on the CNT support or deposited MPc to form hydrogen gas.

density until molecular aggregation starts to occur at high mass loadings. At the optimal methanol-producing potential of −0.94 V, MPcs play an outsized role for HER compared to CNTs. CoPc catalyzes HER with a turnover frequency (TOF) of 3.2 s^{-1} while NiPc and FePc have lower TOFs of 0.26 and 0.63 s^{-1}, respectively.

In this work, we chose 0.1 M phosphate buffer aqueous solutions (pH 7.2) as the electrolyte for HER studies of MPc/CNT catalysts because it has approximately the same pH value as CO_2-saturated 0.1 M aqueous $KHCO_3$, our normally used electrolyte for CO_2 reduction to methanol [7], at pH 6.8. This allows us to avoid possible interference from CO_2 reduction caused by bicarbonate. We first tested the CO_2 reduction performance of the MPc/CNT catalysts with input mass ratio of 5 wt.% (mass loadings: 2.1% CoPc, 3.1% NiPc, and 3.1% FePc). CoPc/CNT catalyzed CO_2 reduction to CO at −0.55 V. High CO FE (> 90%) was achieved at −0.75 and −0.82 V. At a more negative potential of −0.93 V, methanol was observed as a product with a moderate FE of ~ 25% (Fig. 2(a)). This potential-dependent electrocatalytic behavior of CoPc/CNT is similar to what we have observed for the same catalyst in $KHCO_3$ electrolyte [7]. NiPc/CNT exhibited high CO selectivity at −0.75, −0.82, and −0.94 V, with no methanol detected (Fig. 2(b)). FePc/CNT was also able to produce CO from CO_2 reduction, but with low selectivity (Fig. 2(c)). Although some of the total FEs did not reach 100%, all products were accounted for and the FEs were within a reasonable range for these types of measurements.

To differentiate the roles of MPc vs. CNT in catalyzing HER, we first produced a series of CoPc/CNT materials by systematically varying the amount of CoPc included in the preparation. This varying CoPc-to-CNT input ratio led to varied mass loadings of CoPc on CNT in the resulting hybrid materials with a good linearity (Figs. S1 and S2 in the Elecronic Supplementary Material (ESM)), as measured by inductively coupled plasma mass spectrometry (ICP-MS, Table S1 in the ESM). About half of CoPc was successfully loaded on to the CNT support.

The electroactive loading of CoPc on CNT was measured using cyclic voltammetry (CV). The materials all showed a characteristic pair of redox peaks near 0 V, demonstrating consistent chemical properties. The oxidative peak was integrated for the charge (Fig. 3(a) and Fig. S3 in the ESM) and used to calculate the number of electroactive CoPc molecules. The electroactive loading increased with the mass loading up to 8.5% (input ratio 15 wt.%), with about 36% of loaded CoPc molecules being electrochemically active (Fig. 3(b)). This linearity demonstrates that CoPc can be uniformly well dispersed on the CNT surface and the loaded CoPc molecules are electrically wired to the CNT support [14]. Likely, CoPc dispersion is on the molecular level and the surface coverage increases with the mass loading. The molecules are coupled to the CNT surface by π–π stacking [15]. This result suggests that we can controllably cover the CNT surface with CoPc molecules by adjusting the mass loading, therefore successfully affording a material system for distinguishing CoPc and CNT sites in catalyzing HER. The material with 11.3% of CoPc, however, showed a much smaller electroactive percentage than the trend line predicts. This is likely because of aggregation of the CoPc molecules at this high loading [16], reducing the fraction of exposed sites that are electrochemically active [3, 17]. Our CNTs have a surface area of 180–250 m^2/g, as tested by the manufacturer and in agreement with the calculation of 200 m^2/g reported by Peigney et al. for the average multiwalled CNT [18]. The surface area of a CoPc molecule being about 1.45 nm^2 (Fig. S4 in the ESM) [19, 20], we estimate that CoPc at mass loadings of 8.5% and 11.3% would cover about 52%–72% and 69%–96% of the CNT surface, respectively. Considering that there may be repulsion between CoPc molecules and that they may not distribute perfectly, a saturated loading of about 10% is not unreasonable in this case. Attempted characterization of the CoPc aggregates using scanning electron microscopy (SEM) and transmission electron microscopy with electron dispersive X-ray spectroscopy mapping could not resolve visible aggregation on the scale of 10 nm or larger (Figs. S5(a)–S5(f) in the ESM). We hypothesize that this type of aggregation is on the scale of just several molecules, which is difficult to directly observe with common imaging techniques. Further investigation of this interesting phenomenon is still needed.

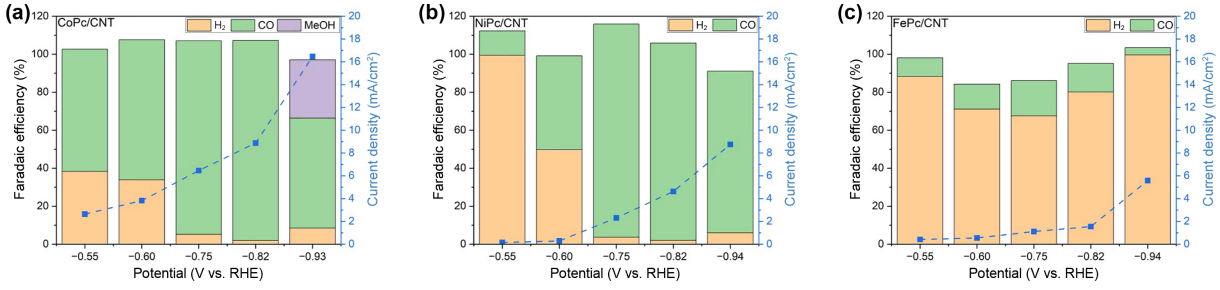

Figure 2 CO_2 reduction of MPc/CNTs: (a) CoPc, (b) NiPc, and (c) FePc. MPc/CNTs were tested in H-cells in CO_2-saturated 0.1 M phosphate buffer electrolyte. Activity was measured via controlled potential electrolysis over several potential steps. The gaseous products quantified via gas chromatography are shown, as well as liquid methanol product from NMR quantification.

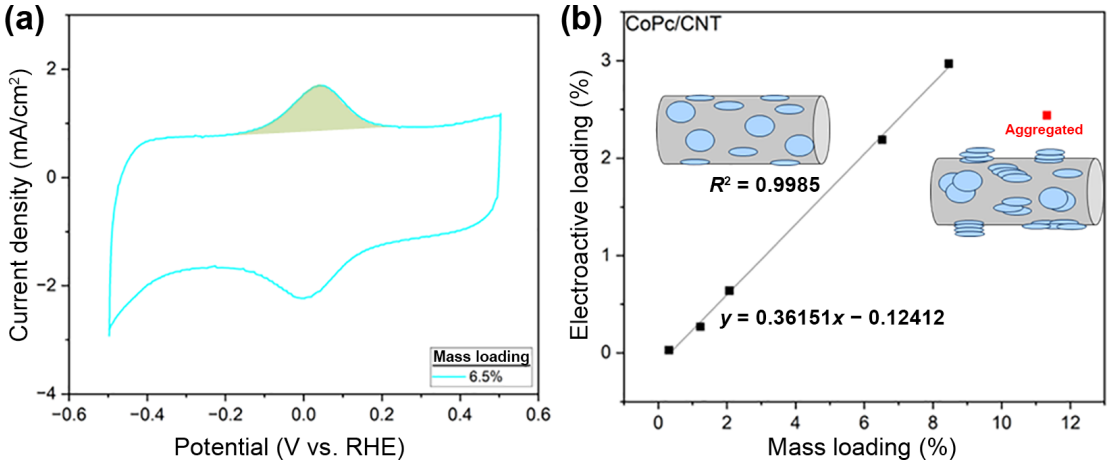

Figure 3 CoPc/CNT electroactive loadings. (a) Cyclic voltammograms were measured for various CoPc/CNT mass loadings, one of which is shown here for 6.5% mass loading (others in Fig. S3 in the ESM). The oxidative peak was integrated for charge which was then used to calculate the number of electroactive molecules. (b) The electroactive loading was plotted against mass loading, with a linear fit excluding the red 11.3% outlier point.

The CoPc/CNT materials with varied CoPc loadings were tested for HER using linear sweep voltammetry (LSV) under Ar flow (Fig. 4(a)). The voltammograms revealed a plateau region where the activity stalled vs. the applied potential (the inset in Fig. 4(a)). It was hypothesized that this range is diffusion-limited for HER, as the proton source near the electrode is depleted faster than new protons can approach. This also indicates that the hydrogen source is first the protons as opposed to abundant water, until more negative potentials where the catalyst is able to perform HER on water [21–23]. To validate this mass transport limitation hypothesis, LSV was scanned with varied stirring speeds (Fig. S6 in the ESM). The increase of the plateau current density with faster stirring supports this interpretation, as more protons are able to reach the electrode surface with the stirring-induced mass transport. In this electrolyte, phosphate acts as a buffer to the proton concentration that is being depleted by reduction [22]. Testing the reaction in different electrolytes, including 0.1 M aqueous $KHCO_3$, K_2SO_4, and KCl, also supported these hypotheses of proton-first reduction and mass transport limitation (Fig. S7 in the ESM). In the aprotic electrolytes K_2SO_4 and KCl, the voltammograms did not manifest a plateau region, instead having a sharp onset of water reduction due to their inability to create protic species in solution [24]. $KHCO_3$ exhibited diffusion limitation but with a less pronounced effect of a gradual slope than the phosphate buffer electrolyte. This is likely because bicarbonate is a weaker proton donor than biphosphate [9].

The HER rates (i.e., current densities) at certain electrode potentials were extracted from the LSV scans and plotted vs. the CoPc mass loadings (Fig. 4(b)). The HER current was relatively independent of mass loading at −0.55 and −0.6 V because the reaction rate was controlled by the diffusion of proton species. At more negative potentials of −0.75, −0.82 and −0.94 V, which are relevant to CO_2 reduction to CO or methanol, the current density increased with higher mass loading (Fig. 4(b)), demonstrating the role of the CoPc molecule in catalyzing HER more favorably than CNTs. The near-linear relationship between current density and CoPc loading again supports good dispersion and electrical wiring of CoPc on CNT. From the slopes of the current density vs. mass loading lines, we were able to derive the HER activity of CoPc molecules with respect to the CNT surface.

Similar to CoPc/CNT, NiPc/CNT and FePc/CNT materials with varied MPc mass loadings were prepared (Table S1 in the ESM) and studied for HER catalysis (Figs. S8(a) and S8(c) in the ESM). Both showed less pronounced diffusion-controlled behavior in the medium overpotential range, possibly because NiPc and FePc are less active than CoPc. As a result, their current density vs. mass loading curves were mostly linear at all the examined potentials

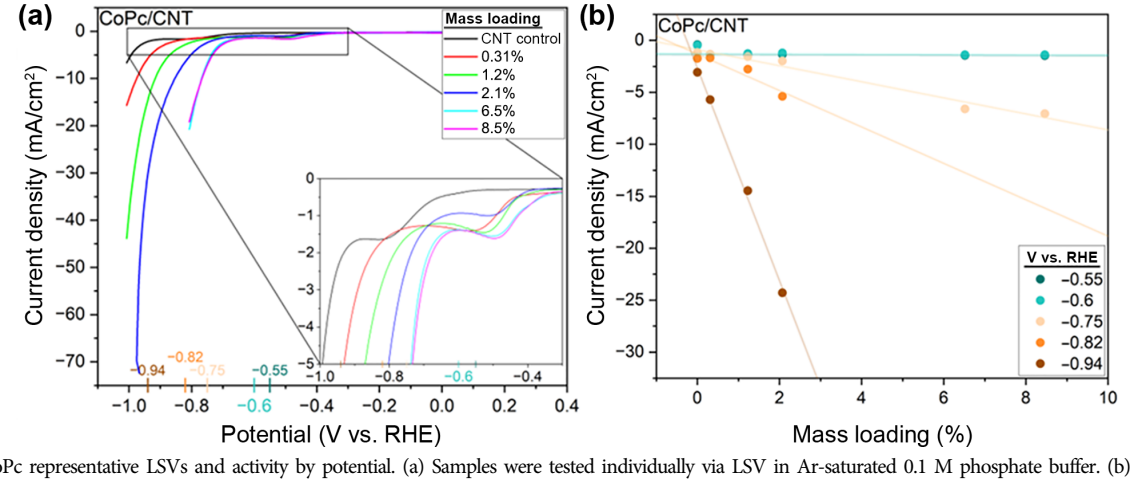

Figure 4 CoPc representative LSVs and activity by potential. (a) Samples were tested individually via LSV in Ar-saturated 0.1 M phosphate buffer. (b) The current densities at selected potentials were extracted and plotted versus mass loading.

(Figs. S8(b) and S8(d) in the ESM). Tafel analysis (Fig. S9 in the ESM) resulted in slopes around 120 mV/dec or larger for all the MPc/CNT materials as well as the CNT control, indicating that their mechanisms are similarly limited by the initial Volmer step of HER [9, 25, 26]. It is interesting to note that NiPc/CNT exhibited linear activity at lower loadings but the activity plateaued after 3.1% (Fig. S8(b) in the ESM), indicating a saturation of its HER catalytic activity. This may be due to earlier aggregation of NiPc molecules; although, like the CoPc/CNT materials, SEM could not visually resolve aggregates (Figs. S5(g) and S5(h) in the ESM). NiPc's tendency to aggregate at lower loading may be related to stronger intermolecular interactions, as indicated by its poorer solubility in N,N-dimethylformamide (DMF) than CoPc and FePc [27], causing molecules to self-assemble in solution or on the CNT surface.

The slopes of current density versus mass loading were used to calculate TOF of the MPcs for HER on CNT (Fig. 5 and Table S2 in the ESM). The TOF for CNT alone was calculated per MPc-equivalent footprint of 1.45 nm^2, the approximate surface area occupied by an MPc molecule (Fig. S4 in the ESM). CoPc had the highest activity for HER out of the MPcs. Although NiPc and FePc were less active, the MPcs were generally more active for HER than the nanotube supports. This difference was more pronounced at more negative potentials. In the context of their CO_2 reduction abilities, the more HER-active CoPc is also the only one of the molecules to produce methanol [7]. These activities might be related, as both demonstrate CoPc's capacity to pull protons from solution and combine them with a bound intermediate. In contrast, NiPc's reduction of CO_2 to CO proceeds with very high selectivity, with little HER side-reactivity [12, 28].

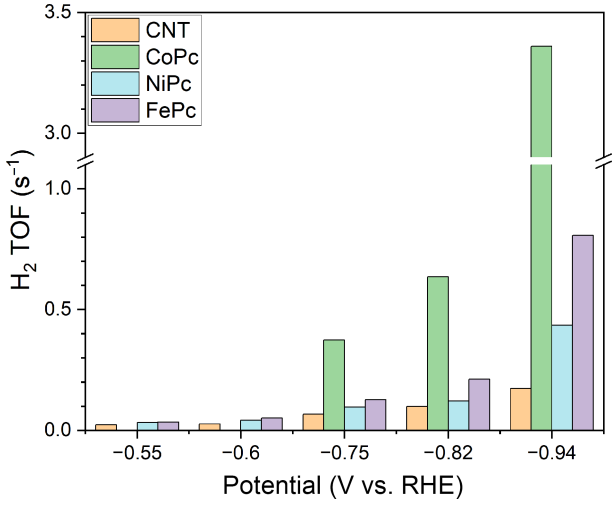

Figure 5 H_2 TOFs of the MPcs on CNT. Activities were calculated using the slope of the current density vs. loading plots. Plain CNT activity was calculated per MPc molecule-equivalent footprint. The values are tabulated in Table S2 in the ESM.

In summary, we demonstrated that the HER activity of MPc/CNT hybrid materials is mainly catalyzed by the MPc rather than the nanotube support. CoPc is the most active for HER, followed by FePc then NiPc. Proton species in the electrolyte are preferentially reduced before water at more positive potentials, leading to a diffusion-limited window of activity. The mass loading of MPc catalyst can be systematically adjusted up to 15 wt.% input with consistent molecular electroactivity. Higher input results in MPc aggregation that is detrimental to catalytic activity.

Electronic Supplementary Material: Supplementary material (additional structural and electrochemical characterization results, ICP-MS results, and TOF analysis) is available in the online version of this article at https://doi.org/10.26599/NR.2026.94908427.

Data availability

All data needed to support the conclusions in the paper are presented in the manuscript and the Electronic Supplementary Material. Additional data related to this paper may be requested from the corresponding author upon request.

Acknowledgements

This work was supported by U.S. National Science Foundation, grant numbers CHE-2154724 (electrocatalysis research) and CBET-2129963 (molecule-nanotube interaction research).

Declaration of competing interest

Author Hailiang Wang is an associate editor of this journal, but he is not involved in the peer-review or decision of this article. The other contributing authors report no conflict of interests in this work.

Author contribution statement

B. T. W.: Experiment design, data collection, data analysis, writing manuscript. C. L. R.: Data collection, experiment design. N. J. H.: Data collection. K. P. Y.: Data collection. Q. S.: Data collection. H. L. W.: Funding acquisition, experiment design, project administration, writing manuscript. All the authors have approved the final manuscript.

Use of AI statement

None.

References

[1] Yang, S. X.; Yu, Y. H.; Gao, X. J.; Zhang, Z. P.; Wang, F. Recent advances in electrocatalysis with phthalocyanines. *Chem. Soc. Rev.* **2021**, *50*, 12985–13011.

[2] Wu, Y. S.; Liang, Y. Y.; Wang, H. L. Heterogeneous molecular catalysts of metal phthalocyanines for electrochemical CO_2 reduction reactions. *Acc. Chem. Res.* **2021**, *54*, 3149–3159.

[3] Liu, J. J.; Yang, J. R.; Dou, Y. H.; Liu, X. W.; Chen, S. H.; Wang, D. S. Deactivation mechanism and mitigation strategies of single-atom site electrocatalysts. *Adv. Mater.* **2025**, *37*, 2420383.

[4] Zhang, X.; Wu, Z. S.; Zhang, X.; Li, L. W.; Li, Y. Y.; Xu, H. M.; Li, X. X.; Yu, X. L.; Zhang, Z. S.; Liang, Y. Y. et al. Highly selective and active CO_2 reduction electrocatalysts based on cobalt phthalocyanine/carbon nanotube hybrid structures. *Nat. Commun.* **2017**, *8*, 14675.

[5] Lu, X.; Wu, Y. S.; Yuan, X. L.; Huang, L.; Wu, Z. S.; Xuan, J.; Wang, Y. F.; Wang, H. L. High-performance electrochemical CO_2 reduction cells based on non-noble metal catalysts. *ACS Energy Lett.* **2018**, *3*, 2527–2532.

[6] Kapusta, S.; Hackerman, N. Carbon dioxide reduction at a metal phthalocyanine catalyzed carbon electrode. *J. Electrochem. Soc.* **1984**, *131*, 1511–1514.

[7] Wu, Y. S.; Jiang, Z.; Lu, X.; Liang, Y. Y.; Wang, H. L. Domino electroreduction of CO_2 to methanol on a molecular catalyst. *Nature* **2019**, *575*, 639–642.

[8] Su, J. J.; Musgrave, C. B.; Song, Y.; Huang, L. B.; Liu, Y.; Li, G.;

Xin, Y. E.; Xiong, P.; Li, M. M. J.; Wu, H. R. et al. Strain enhances the activity of molecular electrocatalysts via carbon nanotube supports. *Nat. Catal.* **2023**, *6*, 818–828.

[9] Li, J.; Shang, B.; Gao, Y. Z.; Cheon, S.; Rooney, C. L.; Wang, H. L. Mechanism-guided realization of selective carbon monoxide electroreduction to methanol. *Nat. Synth.* **2023**, *2*, 1194–1201.

[10] Chang, Q. W.; Liu, Y. M.; Lee, J. H.; Ologunagba, D.; Hwang, S.; Xie, Z. H.; Kattel, S.; Lee, J. H.; Chen, J. G. Metal-coordinated phthalocyanines as platform molecules for understanding isolated metal sites in the electrochemical reduction of CO_2. *J. Am. Chem. Soc.* **2022**, *144*, 16131–16138.

[11] Chen, K. J.; Cao, M. Q.; Lin, Y. Y.; Fu, J. W.; Liao, H. X.; Zhou, Y. J.; Li, H. M.; Qiu, X. Q.; Hu, J. H.; Zheng, X. S. et al. Ligand engineering in nickel phthalocyanine to boost the electrocatalytic reduction of CO_2. *Adv. Funct. Mater.* **2022**, *32*, 2111322.

[12] Zhang, X.; Wang, Y.; Gu, M.; Wang, M. Y.; Zhang, Z. S.; Pan, W. Y.; Jiang, Z.; Zheng, H. Z.; Lucero, M.; Wang, H. L. et al. Molecular engineering of dispersed nickel phthalocyanines on carbon nanotubes for selective CO_2 reduction. *Nat. Energy* **2020**, *5*, 684–692.

[13] Li, X. X.; Chai, G. L.; Xu, X.; Liu, J. J.; Zhong, Z.; Cao, A. H.; Tao, Z. J.; You, W. F.; Kang, L. T. Electrocatalytic reduction of CO_2 to CO over iron phthalocyanine-modified graphene nanocomposites. *Carbon* **2020**, *167*, 658–667.

[14] Li, H.; Jiang, Z.; Yuan, Y. B.; Tang, Y. R.; Zao, J.; Zhang, W. T.; Han, P. Y.; Zhang, X.; Chen, B. L.; Liang, Y. Y. Multiscale engineering of molecular electrocatalysts for the rapid hydrogen evolution reaction. *Nano Res.* **2024**, *17*, 6026–6031.

[15] Rooney, C. L.; Lyons, M.; Wu, Y. S.; Hu, G. F.; Wang, M. Y.; Choi, C.; Gao, Y. Z.; Chang, C. W.; Brudvig, G. W.; Feng, Z. X. et al. Active sites of cobalt phthalocyanine in electrocatalytic CO_2 reduction to methanol. *Angew. Chem., Int. Ed.* **2024**, *63*, e202310623.

[16] Cheon, S.; Li, J.; Wang, H. L. *In situ* generated CO enables high-current CO_2 reduction to methanol in a molecular catalyst layer. *J. Am. Chem. Soc.* **2024**, *146*, 16348–16354.

[17] Du, Y. P.; Mu, X. Q.; Wang, S. C.; Zhang, Y. F.; Chen, F. J.; Zhang, M. Y.; Li, J. L.; Cao, P. P.; Yuan, J. Y.; Zhang, Y. et al. Atomically dispersed catalysts: For the efficient and stable industrial electrosynthesis of H_2O_2. *Energy Environ. Sci.* **2025**, *18*, 5833–5867.

[18] Peigney, A.; Laurent, C.; Flahaut, E.; Bacsa, R. R.; Rousset, A. Specific surface area of carbon nanotubes and bundles of carbon nanotubes. *Carbon* **2001**, *39*, 507–514.

[19] Al-Shewiki, R. K.; Weheabby, S.; Uhlig, N.; Korb, M.; Pester, T.; Zahn, S.; Grecchi, S.; Mussini, P. R.; Rüffer, T.; Lang, H. Cobalt(III)-containing penta-dentate "helmet"-type phthalogens: Synthesis, solid-state structures and their thermal and electrochemical characterization. *Dalton Trans.* **2024**, *53*, 3836–3854.

[20] *Cambridge Structural Database (CSD)* [Online]. Cambridge Crystallographic Data Centre. https://llas.cas.cn/sourcedb/resource/202501/t20250106_308080.html.

[21] Choi, C.; Kwon, S.; Gao, Y. Z.; Cheon, S.; Li, J.; Menges, F.; Goddard III, W. A.; Wang, H. L. CO_2-promoted electrocatalytic reduction of chlorinated hydrocarbons. *J. Am. Chem. Soc.* **2024**, *146*, 8486–8491.

[22] Ooka, H.; Figueiredo, M. C.; Koper, M. T. M. Competition between hydrogen evolution and carbon dioxide reduction on copper electrodes in mildly acidic media. *Langmuir* **2017**, *33*, 9307–9313.

[23] Strmcnik, D.; Uchimura, M.; Wang, C.; Subbaraman, R.; Danilovic, N.; van der Vliet, D.; Paulikas, A. P.; Stamenkovic, V. R.; Markovic, N. M. Improving the hydrogen oxidation reaction rate by promotion of hydroxyl adsorption. *Nat. Chem.* **2013**, *5*, 300–306.

[24] Zhang, Y.; Wan, W. K.; Peng, Y. D.; Guo, Y. J.; Zhou, J. L.; Wang, S. C.; Yuan, J. Y.; Liao, Y. R.; Liu, L. S.; Zhang, Y. F. et al. Corrosion-resistant single-atom catalysts for direct seawater electrolysis. *Natl. Sci. Rev.* **2025**, *12*, nwaf060.

[25] Wan, C. Z.; Ling, Y. S.; Wang, S. B.; Pu, H. T.; Huang, Y.; Duan, X. F. Unraveling and resolving the inconsistencies in tafel analysis for hydrogen evolution reactions. *ACS Cent. Sci.* **2024**, *10*, 658–665.

[26] Cao, P. P.; Mu, X. Q.; Chen, F. J.; Wang, S. C.; Liao, Y. R.; Liu, H.; Du, Y. P.; Li, Y. X.; Peng, Y. D.; Gao, M. Z. et al. Breaking symmetry for better catalysis: Insights into single-atom catalyst design. *Chem. Soc. Rev.* **2025**, *54*, 3848–3905.

[27] Ghani, F.; Kristen, J.; Riegler, H. Solubility properties of unsubstituted metal phthalocyanines in different types of solvents. *J. Chem. Eng. Data* **2012**, *57*, 439–449.

[28] Liu, J. J.; Wei, Z. X.; Gong, Z. C.; Yan, M. M.; Hu, Y. F.; Zhao, S. L.; Ye, G. L.; Fei, H. L. Single-atom CoN_4 sites with elongated bonding induced by phosphorus doping for efficient H_2O_2 electrosynthesis. *Appl. Catal. B: Environ.* **2023**, *324*, 122267.